energies

MDPI

Article

Power, Efficiency, Power Density and Ecological Function Optimization for an Irreversible Modified Closed Variable-Temperature Reservoir Regenerative Brayton Cycle with One Isothermal Heating Process

Lingen Chen [1,2,*], Chenqi Tang [3], Huijun Feng [1,2] and Yanlin Ge [1,2]

1 Institute of Thermal Science and Power Engineering, Wuhan Institute of Technology, Wuhan 430205, China; huijunfeng@139.com (H.F.); geyali9@hotmail.com (Y.G.)
2 School of Mechanical & Electrical Engineering, Wuhan Institute of Technology, Wuhan 430205, China
3 College of Power Engineering, Naval University of Engineering, Wuhan 430033, China; tangchenqi7@163.com
* Correspondence: lgchenna@yahoo.com or lingenchen@hotmail.com; Tel.: +86-27-8361-5046; Fax: +86-27-83638709

Received: 28 July 2020; Accepted: 30 September 2020; Published: 2 October 2020

Abstract: One or more isothermal heating process was introduced to modify single and regenerative Brayton cycles by some scholars, which effectively improved the thermal efficiency and significantly reduced the emissions. To analyze and optimize the performance of this type of Brayton cycle, a regenerative modified Brayton cycle with an isothermal heating process is established in this paper based on finite time thermodynamics. The isothermal pressure drop ratio is variable. The irreversibilities of the compressor, turbine and all heat exchangers are considered in the cycle, and the heat reservoirs are variable-temperature ones. The function expressions of four performance indexes; that is, dimensionless power output, thermal efficiency, dimensionless power density and dimensionless ecological function are obtained. With the dimensionless power density as the optimization objective, the heat conductance distributions among all heat exchangers and the thermal capacitance rate matching among the working fluid and heat reservoir are optimized. Based on the NSGA-II algorithm, the cycle's double-, triple- and quadruple-objective optimization are conducted with the total pressure ratio and the heat conductance distributions among heat exchangers as design variables. The optimal value is chosen from the Pareto frontier by applying the LINMAP, TOPSIS and Shannon entropy methods. The results show that when the pressure ratio in the compressor is less than 12.0, it is beneficial to add the regenerator to improve the cycle performance; when the pressure ratio is greater than 12.0, adding the regenerator will reduce the cycle performance. For single-objective optimization, the four performance indexes could be maximized under the optimal pressure ratios, respectively. When the pressure ratio is greater than 9.2, the cycle is simplified to a closed irreversible simple modified Brayton cycle with one isothermal heating process and coupled to variable-temperature heat reservoirs. Therefore, when the regenerator is used, the range of pressure ratio is limited, and a suitable pressure ratio should be selected. The triple objective (dimensionless power output, dimensionless power density and dimensionless ecological function) optimization' deviation index gained by LINMAP or TOPSIS method is the smallest. The optimization results gained in this paper could offer some new pointers for the regenerative Brayton cycles' optimal designs.

Keywords: finite time thermodynamics; regenerative Brayton cycle with the isothermal heating process; power output; thermal efficiency; power density; ecological function; multi-objective optimization

1. Introduction

Gas turbine plant (Brayton cycle (BCY)) has the characteristics of high safety, high efficiency and high energy density, and is widely used in the fields of thermal power generation, aviation propulsion, pipeline transportation, distributed energy and ship power plant, etc. However, NOx in gas turbine emission pollutants causes serious environmental pollution. The concentration of NOx in pollutants is closely related to the temperature of the combustion. For this reason, Vecchiarelli et al. [1] introduced an isothermal heating process (IHP) into the BCY, which effectively improved the thermal efficiency (TEF) and significantly reduced the emissions. The regenerative BCYs with IHP were studied by using the classical thermodynamics in [2–4]. El-Maksoud [5] added two IHPs in a binary BCY, and the cycle performance was significantly improved.

The temperature difference between the working fluid (WF) and the heat reservoir is not considered in the classical thermodynamic analysis. Compared to the classical thermodynamics, the finite size device and the finite time process of the finite rate heat exchange between the system and the environment are considered in the finite time thermodynamics (FTT) [6] and see the books by Berry et al. [7], Dincer et al. [8], Perescu et al. [9], Kaushik et al. [10] and Sieniutycz [11], as well as the review papers by Chen et al. [12], Andresen [13], Roach et al. [14] and Feidt et al. [15]. Berry et al. [7] comprehensively summarized the previous nearly 20 years' achievements on the FTT and optimal control. Dincer et al. [8] studied all kinds of advanced multi-output thermodynamic cycles and found that compared with traditional thermodynamic cycles, the advanced cycles had higher sustainability and energy utilization efficiency. Perescu et al. [9] studied how to meet the electricity and hot water needed for the personal housing by designing suitable mirrors. By using the FTT, Kaushik et al. [10] studied Carnot, Rankine, Brayton, Stirling, Ericsson Cycles, etc. Sieniutycz [11] described the properties of complexity and complex thermo-economic systems. Chen et al. [12] discussed the performance optimization of the thermodynamic processes and devices under the constraint of finite time or finite size. Andresen [13] introduced the development of the FTT in the past ten years and focused on the methods that he considered to be the most promising. Roach et al. [14] discussed the application of the principles of the FTT and control thermodynamics to biological processes. Feidt et al. [15] suggested discussing the heat transfer entropy and the production of entropy to study the external or internal irreversibility of the converter. The FTT has been widely used in thermodynamic cycle researches, the power output [16–18], TEF [16–18], power density [19–23] and ecological function [24–28] are often targeted when applying FTT to analyze or optimize the cycle performances.

Kaushik et al. [29] applied FTT in the study of the regenerative BCY with an IHP and found that compared with the traditional BCY, the TEF of the new BCY was significantly improved. Based on this, Tyagi et al. [30–35] and Kumar et al. [36] analyzed and optimized the regenerative [30,32,36], intercooled regenerative [31,33] and complex [34,35] BCYs with IHPs. With dimensionless power output (DPO), TEF, dimensionless power density (DPD) [37] and dimensionless ecological function (DEF) [38] as the objectives, Wang et al. [37,38] analyzed an endoreversible BCY modified by isothermal heating and found that the power density and ecological function are the trade-offs between power output and TEF. Based on this, Tang et al. [39,40] further applied the NSGA-II algorithm to optimize an endoreversible cycle and carried out sensitivity analysis. Arora et al. [41,42] analyzed and optimized a regenerative BCY with an IHP. Based on [5], Qi et al. [43] analyzed a binary BCY with two IHPs, derived the expression of DPO and TEF, and found that the DPO can be maximized by choosing an optimal pressure ratio. Tang et al. [44] took the DPO as the objective and the heat conductance distributions (HCDs) as design variables to optimize a closed binary Brayton with IHPs.

FTT will be applied to establish a model of closed regenerative BCY with an IHP and variable-temperature heat reservoirs in this paper. The isothermal pressure drop ratio (IPDR) is variable. The DPO, TEF, DPD and DEF will be obtained, and the influences of the regenerator's effectiveness on the performance indexes will be analyzed. Taking the DPD as an example, the optimal HCDs among heat exchangers under maximum DPD will be gained. Based on the NSGA-II algorithm, the DPO, TEF, DPD and DEF will be maximized and the corresponding Pareto frontier will be obtained.

The optimal value will be chosen from the Pareto frontier by applying the LINMAP, TOPSIS and Shannon entropy methods.

2. Cycle Model

The schematic and *T-s* diagrams of a closed irreversible regenerative modified BCY with an IHP and coupled to variable-temperature heat reservoirs (VTHRs) are shown in Figures 1 and 2, respectively. A compressor (C), a regenerator, a regular combustion chamber (RCC), a converging combustion chamber (CCC), a turbine (T) and a precooler are the main components of the cycle. The cycle consists of an irreversible adiabatic compression process (process 1–2), two isobaric heat absorption processes (processes 2–3 and 3–4), an IHP (process 4–5), an irreversible adiabatic expansion process (process 5–6) and two isobaric exothermic processes (processes 6–7 and 7–1). The processes of 1–2 s and 5–6 s are the corresponding isentropic processes.

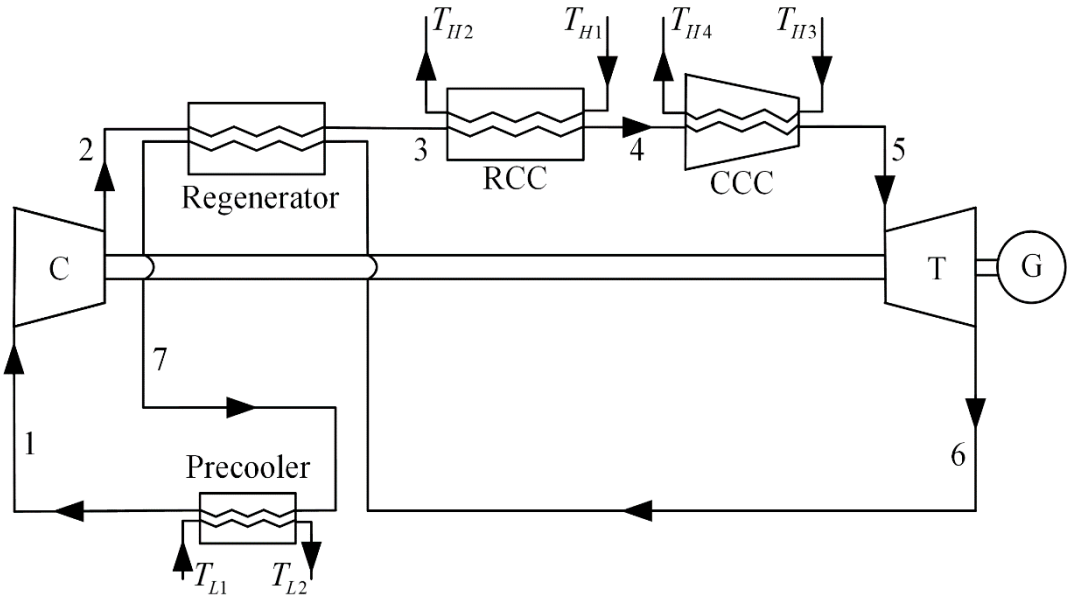

Figure 1. Schematic diagram of the cycle.

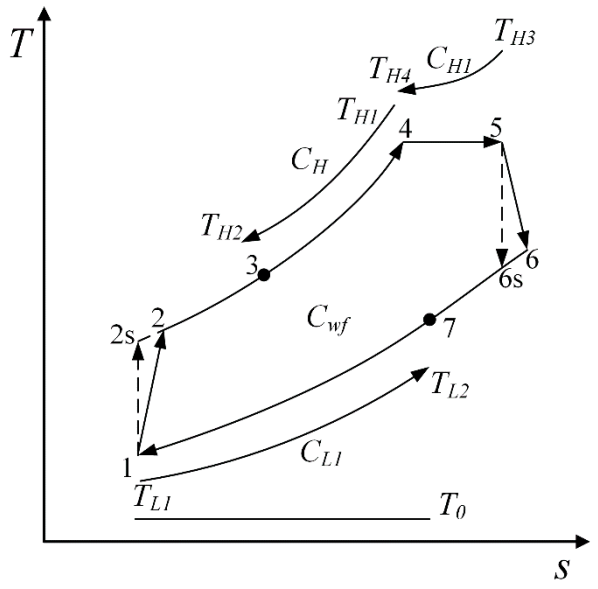

Figure 2. *T-s* diagram of the cycle.

It is assumed that the WF is a compressible ideal gas. The temperature of the WF gradually increases as it flows through a heating pipeline at subsonic speeds; the temperature decreases as it flows through a pipeline with a decreasing cross-sectional area and without heating at subsonic speeds. Combined with the two points, the convergent pipeline can be precisely and appropriately adjusted to achieve the isothermal heating of the WF [1]. Thus, the WF is isothermally heated in the CCC, and the thermal energy absorbed by the WF is converted into the kinetic energy.

The thermal capacitance rates of the WF and outer fluids at the RCC, CCC and precooler are C_{wf}, C_H, C_{H1} and C_L, respectively. The dimensionless maximum specific capacity is v_5/v_1. The heat conductances of the regenerator, RCC, CCC and precooler are U_R, U_H, U_{H1} and U_L, the numbers of heat transfer units are N_R, N_H, N_{H1} and N_L, and the effectivenesses of the heat exchangers' are E_R, E_H, E_{H1} and E_L, respectively. The corresponding expressions are:

$$N_R = U_R/C_{wf},\ N_H = U_H/C_{Hmin},\ N_{H1} = U_{H1}/C_{H1},\ N_L = U_L/C_{Lmin} \tag{1}$$

$$E_R = N_R/(N_R+1) \tag{2}$$

$$E_H = \frac{1-\exp[-N_H(1-C_{Hmin}/C_{Hmax})]}{1-(C_{Hmin}/C_{Hmax})\exp[-N_H(1-C_{Hmin}/C_{Hmax})]} \tag{3}$$

$$E_{H1} = 1-\exp(-N_{H1}) \tag{4}$$

$$E_L = \frac{1-\exp[-N_L(1-C_{Lmin}/C_{Lmax})]}{1-(C_{Lmin}/C_{Lmax})\exp[-N_L(1-C_{Lmin}/C_{Lmax})]} \tag{5}$$

where $C_{Hmax} = max\{C_{wf}, C_H\}$, $C_{Hmin} = min\{C_{wf}, C_H\}$, $C_{Lmax} = max\{C_{wf}, C_L\}$ and $C_{Lmin} = min\{C_{wf}, C_L\}$.

When $C_{Hmax} = C_{Hmin}$ or $C_{Lmax} = C_{Lmin}$, Equations (3) and (5) are simplified as:

$$E_H = N_H/(N_H+1) \tag{6}$$

$$E_L = N_L/(N_L+1) \tag{7}$$

Processes 1–2s and 5–6s are the isentropic processes, so there are:

$$T_{2s}/T_1 = \pi^m = x \tag{8}$$

$$T_5/T_{6s} = \pi^m \pi_t^m = xy \tag{9}$$

where $m = (k-1)/k$ and k is the ratio of specific heats.

For the IHP of process 4–5, one has:

$$T_4 = T_5 \tag{10}$$

$$\dot{Q}_{4-5} = \dot{m}(h_5 - h_4) - \dot{m}\int_4^5 vdp = -\dot{m}R_g T_4 \ln \pi_t \tag{11}$$

where $\dot{m}$ is the mass flow rate, h is the specific enthalpy, $\pi_t (= p_5/p_4 \le 1)$ is the IPDR, and $\dot{Q}_{4-5}$ is heat transfer rate. The degree of isothermal heating can be measured by the value of π_t. Simultaneously, π_t satisfies the following constraints:

$$\pi^{-1} \le \pi_t \le 1,\ \pi_t = \exp[\frac{-c_p(k-1)(M_5^2 - M_4^2)}{2R_g}] \tag{12}$$

The velocity of the WF must be subsonic, i.e., $M_5 \le 1$. Considering that the WF has an initial velocity, $M_4 = 0.2$ and $M_5 = 1$, thus $(M_5^2 - M_4^2)_{\max} = 0.96$ and $(\pi_t)_{\min} = 0.5107$ can be obtained.

The irreversibilities in the compressor and turbine are considered. The efficiencies of them are:

$$\eta_c = (T_{2s} - T_1)/(T_2 - T_1) \tag{13}$$

$$\eta_t = (T_5 - T_6)/(T_5 - T_{6s}) \tag{14}$$

The heat transfer rate ($\dot{Q}_{2-3}$) at the regenerator, heat-absorbing rates ($\dot{Q}_{3-4}$ and $\dot{Q}_{4-5}$) at the RCC and CCC and heat-releasing rate ($\dot{Q}_{5-1}$) at the precooler are, respectively:

$$\dot{Q}_{2-3} = C_{wf}(T_3 - T_2) = C_{wf}(T_6 - T_7) = C_{wf}E_R(T_6 - T_2) \tag{15}$$

$$\dot{Q}_{3-4} = C_{wf}(T_4 - T_3) = C_H(T_{H1} - T_{H2}) = C_{Hmin}E_H(T_{H1} - T_3) \tag{16}$$

$$\dot{Q}_{4-5} = \dot{m}(V_5^2 - V_4^2)/2 = C_{H1}(T_{H3} - T_{H4}) = C_{H1}E_{H1}(T_{H3} - T_4) \tag{17}$$

$$\dot{Q}_{7-1} = C_{wf}(T_7 - T_1) = C_L(T_{L2} - T_{L1}) = C_{Lmin}E_L(T_7 - T_{L1}) \tag{18}$$

The power output (W), TEF (η), power density (P), entropy production rate (s_g) and ecological function (E) are, respectively, calculated as:

$$W = \dot{Q}_{3-4} + \dot{Q}_{4-5} - \dot{Q}_{7-1} \tag{19}$$

$$\eta = W/\left(\dot{Q}_{3-4} + \dot{Q}_{4-5}\right) \tag{20}$$

$$P = W/v_6 \tag{21}$$

$$s_g = C_H \ln(T_{H2}/T_{H1}) + C_{H1} \ln(T_{H4}/T_{H3}) + C_L \ln(T_{L2}/T_{L1}) \tag{22}$$

$$E = W - T_0 s_g \tag{23}$$

where T_0 is the ambient temperature.

In combination with Equations (8)–(10) and Equations (13)–(18), the analytical expressions of the state points' temperatures are:

$$T_3 = a_1 = \frac{\begin{array}{c} C_{Lmin}C_{wf}E_LT_{L1}xy(E_R-1)(\eta_c+x-1) - C_{Hmin}E_HT_{H1}[xy(\eta_t-1)- \\ \eta_t]\left\{C_{wf}[E_R(\eta_c+2x-2)-\eta_c-x+1] - C_{Lmin}E_L(2E_R-1)(\eta_c+ \right. \\ \left. x-1)\right\} \end{array}}{\begin{array}{c} C_{Hmin}C_{Lmin}E_HE_L(2E_R-1)(\eta_c+x-1)[xy(\eta_t-1)-\eta_t] - C_{Hmin}C_{wf} \\ E_H[E_R(\eta_c+2x-2)-\eta_c-x+1][xy(\eta_t-1)-\eta_t] + C_{Lmin}C_{wf}E_L \\ (\eta_c+x-1)[xy(E_R+\eta_t-2E_R\eta_t-1)+\eta_t(2E_R-1)] + C_{wf}^2\{\eta_t(x \\ y-1)[E_R(\eta_c+2x-2)-\eta_c-x+1] + xy(E_R+x-1-xE_R)\} \end{array}} \tag{24}$$

$$T_1 = a_2 = \frac{a_1\eta_c(E_R-1)(C_{wf}-C_{Lmin}E_L) - C_{Lmin}E_LE_R\eta_cT_{L1}}{C_{wf}[E_R(\eta_c+2x-2)-\eta_c-x+1] - C_{Lmin}E_L(2E_R-1)(\eta_c+x-1)} \tag{25}$$

$$T_{L2} = a_3 = \frac{\begin{array}{c} C_{Lmin}E_L\left\{C_{wf}\eta_c(E_R-1)(a_1-T_{L1}) - C_LT_{L1}(2E_R-1)(\eta_c+x-1) + C_{wf}T_{L1} \right. \\ \left. [x-1-2E_R(x-1)]\right\} + C_LC_{wf}T_{L1}[E_R(\eta_c+2x-2)-\eta_c-x+1] \end{array}}{C_L\left\{C_{wf}[E_R(\eta_c+2x-2)-\eta_c-x+1] - C_{Lmin}E_L(2E_R-1)(\eta_c+x-1)\right\}} \tag{26}$$

$$T_2 = \frac{(x+\eta_c-1)[a_1\eta_c(C_{wf}-C_{Lmin}E_L)(E_R-1) - C_{Lmin}E_LE_R\eta_cT_{L1}]}{\eta_c\left\{C_{wf}[E_R(\eta_c+2x-2)-\eta_c-x+1] - C_{Lmin}E_L(2E_R-1)(x+\eta_c-1)\right\}} \tag{27}$$

$$T_{2s} = \frac{x[a_1\eta_c(E_R-1)(C_{wf}-C_{Lmin}E_L) - C_{Lmin}E_LE_R\eta_cT_{L1}]}{C_{wf}[E_R(\eta_c+2x-2)-\eta_c-x+1] - C_{Lmin}E_L(2E_R-1)(\eta_c+x-1)} \tag{28}$$

$$T_4 = T_5 = \frac{C_{Hmin}E_H a_1 + C_{Hmin}E_H T_{H1} + C_{wf}a_1}{C_{wf}} \tag{29}$$

$$T_6 = \frac{(E_R-1)(\eta_c+x-1)[a_1\eta_c(E_R-1)(C_{wf}-C_{Lmin}E_L)-C_{Lmin}E_L E_R\eta_c T_{L1}]}{E_R\eta_c\left\{C_{wf}[E_R(\eta_c+2x-2)-\eta_c-x+1]-C_{Lmin}E_L(2E_R-1)(\eta_c+x-1)\right\}} + \frac{a_1}{E_R} \tag{30}$$

$$T_{6s} = \frac{a_1(C_{wf}-C_{Hmin}E_H)+C_{Hmin}E_H T_{H1}}{C_{wf}xy} \tag{31}$$

$$T_7 = \frac{(2E_R-1)(\eta_c+x-1)[a_1\eta_c(E_R-1)(C_{wf}-C_{Lmin}E_L)-C_{Lmin}E_L E_R\eta_c T_{L1}]}{\eta_c E_R\left\{C_{wf}[E_R(\eta_c+2x-2)-\eta_c-x+1]-C_{Lmin}E_L(2E_R-1)(\eta_c+x-1)\right\}} + \frac{a_1(1-E_R)}{E_R} \tag{32}$$

$$T_{H2} = \frac{C_H T_{H1} + C_{Hmin}E_H a_1 - C_{Hmin}E_H T_{H1}}{C_H} \tag{33}$$

$$T_{H4} = \frac{E_{H1}[C_{Hmin}E_H(T_{H1}-a_1)+C_{wf}(a_1-T_{H3})]}{C_{wf}} + T_{H3} \tag{34}$$

By substituting Equations (24)–(34) into Equations (19)–(23), the DPO ($\overline{W}$), DPD ($\overline{P}$) and DEF ($\overline{E}$) can be obtained, as follows:

$$\overline{W} = \frac{W}{C_{wf}T_0} = \frac{\begin{array}{c}C_{H1}C_{Hmin}E_H E_{H1}E_R\eta_c(a_1-T_{H1}) + C_{wf}E_R[C_{Hmin}E_H(T_{H1}-a_1)+C_{H1}E_{H1}\\ (T_{H3}-a_1)]\eta_c + C_{wf}^2\{a_1\eta_c(E_R-1)+a_2[\eta_c+x-1-E_R(\eta_c+2x-2)]\}\end{array}}{C_{wf}^2 E_R\eta_c T_0} \tag{35}$$

$$\eta = \frac{\begin{array}{c}C_{H1}C_{Hmin}E_H E_{H1}E_R\eta_c(T_{H1}-a_1) + C_{wf}E_R\eta_c[C_{Hmin}E_H(T_{H1}-a_1)+C_{H1}E_{H1}\\ (a_1-T_{H3})] + C_{wf}^2\{a_2[1-\eta_c-x+E_R(\eta_c+2x-2)]-a_1\eta_c(E_R-1)\}\end{array}}{E_R\eta_c[C_{Hmin}E_H(C_{wf}-C_{H1}E_{H1})(a_1-T_{H1})+C_{H1}C_{wf}E_{H1}(a_1-T_{H3})]} \tag{36}$$

$$\overline{P} = \frac{\overline{W}}{v_6} = \frac{\begin{array}{c}a_2\Big\{C_{H1}C_{Hmin}E_H E_{H1}E_R\eta_c(T_{H1}-a_1) + C_{wf}E_R\eta_c[C_{Hmin}E_H(a_1-T_{H1})+C_{H1}\\ E_{H1}(a_1-T_{H3})] + C_{wf}^2\{a_2[1-\eta_c-x+E_R(\eta_c+2x-2)]-a_1\eta_c(E_R-1)\}\Big\}\end{array}}{C_{wf}^2 T_0[a_2(E_R-1)(1-\eta_c-x)-a_1\eta_c]} \tag{37}$$

$$\overline{E} = \frac{E}{C_{wf}T_0} = \frac{\begin{array}{c}C_{H1}C_{Hmin}E_H E_{H1}E_R\eta_c(a_1-T_{H1}) + C_{wf}E_R\eta_c[C_{Hmin}E_H(T_{H1}-a_1)\\ +C_{H1}E_{H1}(T_{H3}-a_1)] + C_{wf}^2\{a_1\eta_c(E_R-1)+a_2[\eta_c+x-E_R(\eta_c\\ +2x-2)-1]\}\end{array}}{E_R T_0\eta_c C_{wf}^2} - \frac{\begin{array}{c}C_H\ln[1+C_{Hmin}E_H(a_1-T_{H1})/(C_H T_{H1})] + C_{H1}\ln\{1+E_{H1}[a_1-T_{H3}+C_{Hmin}\\ E_H(T_{H1}-a_1)/C_{wf}]/T_{H3}\Big\} + C_L\ln(a_3/T_{L1})\end{array}}{C_{wf}} \tag{38}$$

The major differences between this paper and the [40] are the following aspects: Firstly, the irreversibilities in the compressor and turbine are considered in this paper; this is also the difference between the endoreversible model and the irreversible one. Secondly, the regenerator is added in this paper, that is, this paper studies the performance of the regenerated cycle, while [40] studied the performance of a simple cycle. Thirdly, the ecological function is studied in this paper. Fourthly, the double, triple or quadruple objective optimization is considered in this paper, but only triple objective optimization is considered in the [40]. Therefore, this paper is significantly different from the [40]. Equations (35)–(38) have a certain universality. When C_H, C_{H1}, C_L, E_{H1}, η_c and η_t are different values, the cycle could be simplified to different special cycles.

When $\eta_c = \eta_t = 1$, Equations (35)–(38) are simplified into $\overline{W}$, η, $\overline{P}$ and $\overline{E}$ of a closed endoreversible regenerative modified BCY with an IHP and coupled to VTHRs:

$$\overline{W} = \frac{\begin{array}{c} C_{H1}C_{Hmin}E_HE_{H1}E_R(a_4 - T_{H1}) + C_{wf}E_R[C_{Hmin}E_H(T_{H1} - a_4) + \\ C_{H1}E_{H1}(T_{H3} - a_4)] + C_{wf}^2\{a_4(E_R - 1) + a_5[x - E_R(2x - 1)]\} \end{array}}{C_{wf}^2E_RT_0} \tag{39}$$

$$\eta = \frac{\begin{array}{c} C_{H1}C_{Hmin}E_HE_{H1}E_R(T_{H1} - a_4) + C_{wf}E_R[C_{Hmin}E_H(T_{H1} - a_4) + \\ C_{H1}E_{H1}(a_4 - T_{H3})] + C_{wf}^2[a_5E_R(2x - 1) - a_4(E_R - 1) - x] \end{array}}{E_R[C_{Hmin}E_H(C_{wf} - C_{H1}E_{H1})(a_4 - T_{H1}) + C_{H1}C_{wf}E_{H1}(a_4 - T_{H3})]} \tag{40}$$

$$\overline{P} = \frac{\begin{array}{c} a_5\Big\{C_{H1}C_{Hmin}E_HE_{H1}E_R(T_{H1} - a_4) + C_{wf}E_R[C_{Hmin}E_H(a_4 - T_{H1}) + \\ C_{H1}E_{H1}(a_4 - T_{H3})] + C_{wf}^2\{a_5[E_R(2x - 1) - x] - a_4(E_R - 1)\} \end{array}}{-C_{wf}^2T_0[a_5x(E_R - 1) + a_4]} \tag{41}$$

$$\overline{E} = \frac{\begin{array}{c} C_{H1}C_{Hmin}E_HE_{H1}E_R(a_4 - T_{H1}) + C_{wf}E_R[C_{Hmin}E_H(T_{H1} - a_4) + C_{H1} \\ E_{H1}(T_{H3} - a_4)] + C_{wf}^2\{a_4(E_R - 1) + a_5[x - E_R(2x - 1)]\} \end{array}}{E_RT_0C_{wf}^2} - \frac{\begin{array}{c} C_H\ln[1 + C_{Hmin}E_H(a_4 - T_{H1})/(C_HT_{H1})] + C_{H1}\ln\{1 + E_{H1}[a_4 - T_{H3} + \\ C_{Hmin}E_H(T_{H1} - a_4)/C_{wf}]/T_{H3}\Big\} + C_L\ln(a_6/T_{L1}) \end{array}}{C_{wf}} \tag{42}$$

where

$$a_4 = \frac{\begin{array}{c} C_{Lmin}C_{wf}E_LT_{L1}xyx(E_R - 1) + C_{Hmin}E_HT_{H1}\Big\{C_{wf}[E_R(2x - 1) - x] - C_{Lmin}E_Lx(2E_R - 1)\Big\} \end{array}}{\begin{array}{c} C_{Hmin}C_{wf}E_H[E_R(2x - 1) - x] - C_{Hmin}C_{Lmin}E_HE_Lx(2E_R - 1) + C_{Lmin}C_{wf}E_Lx[xy(E_R - 2E_R) \\ +(2E_R - 1)] + C_{wf}^2\{(xy - 1)[E_R(2x - 1) - x] + xy(E_R + x - 1 - xE_R)\} \end{array}} \tag{43}$$

$$a_5 = \frac{a_1(E_R - 1)(C_{wf} - C_{Lmin}E_L) - C_{Lmin}E_LE_RT_{L1}}{C_{wf}[E_R(2x - 1) - x] - C_{Lmin}E_Lx(2E_R - 1)} \tag{44}$$

$$a_6 = \frac{\begin{array}{c} C_{Lmin}E_L\Big\{C_{wf}(E_R - 1)(a_1 - T_{L1}) - C_LT_{L1}x(2E_R - 1) + C_{wf} \\ T_{L1}[x - 1 - 2E_R(x - 1)]\} + C_LC_{wf}T_{L1}[E_R(2x - 1) - x] \end{array}}{C_L\Big\{C_{wf}[E_R(2x - 1) - x] - C_{Lmin}E_Lx(2E_R - 1)\Big\}} \tag{45}$$

When $C_H = C_L \to \infty$, Equations (35)–(38) are simplified into $\overline{W}$, η, $\overline{P}$ and $\overline{E}$ of a closed irreversible regenerative modified BCY with an IHP and coupled to constant-temperature heat reservoirs (CTHRs):

$$\overline{W} = \frac{\begin{array}{c} C_{H1}E_HE_{H1}E_R\eta_c(a_7 - T_{H1}) + E_R\eta_c[C_{wf}E_H(T_{H1} - a_7) + C_{H1}E_{H1}(T_{H3} - \\ a_7)] + C_{wf}\{a_7\eta_c(E_R - 1) + a_8[\eta_c + x - 1 - E_R(\eta_c + 2x - 2)]\} \end{array}}{C_{wf}E_R\eta_cT_0} \tag{46}$$

$$\eta = \frac{\begin{array}{c} C_{H1}E_HE_{H1}E_R\eta_c(T_{H1} - a_7) + C_{wf}\{a_8[1 - \eta_c - x + E_R(\eta_c + 2x - 2)] - \\ a_7\eta_c(E_R - 1)\} + E_R\eta_c[C_{wf}E_H(T_{H1} - a_7) + C_{H1}E_{H1}(a_7 - T_{H3})] \end{array}}{E_R\eta_c[E_H(C_{wf} - C_{H1}E_{H1})(a_7 - T_{H1}) + C_{H1}E_{H1}(a_7 - T_{H3})]} \tag{47}$$

$$\overline{P} = \frac{\begin{array}{c} a_8\Big\{C_{H1}E_HE_{H1}E_R\eta_c(T_{H1} - a_7) + E_R\eta_c[C_{wf}E_H(a_7 - T_{H1}) + C_{H1}E_{H1}(a_7 \\ -T_{H3})] + C_{wf}\{a_8[1 - \eta_c - x + E_R(\eta_c + 2x - 2)] - a_7\eta_c(E_R - 1)\}\} \end{array}}{C_{wf}T_0[a_8(E_R - 1)(1 - \eta_c - x) - a_7\eta_c]} \tag{48}$$

$$\overline{E} = \frac{\begin{array}{c} C_{H1}C_{wf}E_HE_{H1}E_R\eta_c(a_7 - T_{H1}) + C_{wf}E_R\eta_c[C_{wf}E_H(T_{H1} - a_7) + C_{H1}E_{H1} \\ (T_{H3} - a_7)] + C_{wf}^2\{a_7\eta_c(E_R - 1) + a_8[\eta_c + x - E_R(\eta_c + 2x - 2) - 1]\} \end{array}}{E_RT_0\eta_cC_{wf}^2} - \frac{\begin{array}{c} C_H \ln[1 + C_{wf}E_H(a_7 - T_{H1})/(C_HT_{H1})] + C_{H1} \ln\{1 + E_{H1}[a_7 - T_{H3} + E_H \\ (T_{H1} - a_7)]/T_{H3}\} + C_L \ln(a_9/T_{L1}) \end{array}}{C_{wf}} \quad (49)$$

where

$$a_7 = \frac{\begin{array}{c} E_LT_{L1}xy(E_R - 1)(\eta_c + x - 1) - E_HT_{H1}[(\eta_t - 1)xy - \eta_t]\{[E_R(\eta_c + 2x - \\ 2) - \eta_c - x + 1] - E_L(2E_R - 1)(\eta_c + x - 1)\} \end{array}}{\begin{array}{c} E_HE_L(2E_R - 1)(\eta_c + x - 1)[(\eta_t - 1)xy - \eta_t] - E_H[E_R(\eta_c + 2x - 2) - \eta_c - x + \\ 1][xy(\eta_t - 1) - \eta_t] + E_L(\eta_c + x - 1)[xy(E_R + \eta_t - 2E_R\eta_t - 1) + \eta_t(2E_R - 1)] + \\ \{\eta_t(xy - 1)[E_R(\eta_c + 2x - 2) - \eta_c - x + 1] + xy(-xE_R + E_R + x - 1)\} \end{array}} \quad (50)$$

$$a_8 = \frac{a_7\eta_c(E_R - 1)(1 - E_L) - E_LE_R\eta_cT_{L1}}{[E_R(\eta_c + 2x - 2) - \eta_c - x + 1] - E_L(2E_R - 1)(\eta_c + x - 1)} \quad (51)$$

$$a_9 = \frac{\begin{array}{c} E_L\Big\{C_{wf}\eta_c(E_R - 1)(a_7 - T_{L1}) - C_LT_{L1}(2E_R - 1)(\eta_c + x - 1) + C_{wf}T_{L1} \\ [x - 1 - 2E_R(x - 1)]\} + C_LT_{L1}[E_R(\eta_c + 2x - 2) - \eta_c - x + 1] \end{array}}{C_L\{[E_R(\eta_c + 2x - 2) - \eta_c - x + 1] - E_L(2E_R - 1)(\eta_c + x - 1)\}} \quad (52)$$

When $C_H = C_L \to \infty$ and $\eta_c = \eta_t = 1$, Equations (35)–(38) are simplified into $\overline{W}$, η, $\overline{P}$ and $\overline{E}$ of a closed endoreversible regenerative modified BCY with an IHP and coupled to CTHRs:

$$\overline{W} = \frac{\begin{array}{c} C_{H1}E_HE_{H1}E_R(a_{10} - T_{H1}) + E_R[C_{wf}E_H(T_{H1} - a_{10}) + C_{H1}E_{H1} \\ (T_{H3} - a_{10})] + C_{wf}\{a_{10}(E_R - 1) + a_{11}[x - E_R(2x - 1)]\} \end{array}}{C_{wf}E_RT_0} \quad (53)$$

$$\eta = \frac{\begin{array}{c} C_{wf}\{a_{11}[E_R(2x - 1) - x] - a_{10}(E_R - 1)\} + E_R[C_{wf}E_H(T_{H1} - \\ a_{10}) + C_{H1}E_{H1}(a_{10} - T_{H3})] + C_{H1}E_HE_{H1}E_R(T_{H1} - a_{10}) \end{array}}{E_R[E_H(C_{wf} - C_{H1}E_{H1})(a_{10} - T_{H1}) + C_{H1}E_{H1}(a_{10} - T_{H3})]} \quad (54)$$

$$\overline{P} = \frac{\begin{array}{c} a_{11}\Big\{C_{H1}E_HE_{H1}E_R(T_{H1} - a_{10}) + E_R[C_{wf}E_H(a_{10} - T_{H1}) + C_{H1} \\ E_{H1}(a_{10} - T_{H3})] + C_{wf}\{a_{11}[E_R(2x - 1) - x] - a_{10}(E_R - 1)\}\} \end{array}}{-C_{wf}T_0[xa_{11}(E_R - 1) + a_{10}\eta_c]} \quad (55)$$

$$\overline{E} = \frac{\begin{array}{c} C_{H1}C_{wf}E_HE_{H1}E_R(a_{10} - T_{H1}) + C_{wf}E_R[C_{wf}E_H(T_{H1} - a_{10}) + C_{H1} \\ E_{H1}(T_{H3} - a_{10})] + C_{wf}^2\{a_{10}(E_R - 1) + a_{11}[x - E_R(2x - 1)]\} \end{array}}{E_RT_0C_{wf}^2} - \frac{\begin{array}{c} \Big\{C_H \ln[1 + C_{wf}E_H(a_{10} - T_{H1})/(C_HT_{H1})] + C_{H1} \ln\{1 + E_{H1}[a_{10} - \\ T_{H3} + C_{wf}E_H(T_{H1} - a_{10})/C_{wf}]/T_{H3}\Big\} + C_L \ln(a_{12}/T_{L1}) \end{array}}{C_{wf}} \quad (56)$$

where

$$a_{10} = \frac{\begin{array}{c} E_LT_{L1}x^2y(E_R - 1) + E_HT_{H1}\{[E_R(2x - 1) - x] - E_Lx(2E_R - 1)\} \end{array}}{\begin{array}{c} E_H[E_R(2x - 1) - x] + \{(xy - 1)[E_R(2x - 1) - x] + xy(1 - x) \\ (E_R - 1)\} + E_Lx[(2E_R - 1) - E_Rxy] - E_HE_Lx(2E_R - 1) \end{array}} \quad (57)$$

$$a_{11} = \frac{a_{10}(E_R - 1)(1 - E_L) - E_LE_RT_{L1}}{E_R(2x - 1) - x - E_Lx(2E_R - 1)} \quad (58)$$

$$a_{12} = \frac{E_L\{C_{wf}(E_R-1)(a_{10}-T_{L1}) - C_L T_{L1} x(2E_R-1) + C_{wf} T_{L1}(x-1)(1-2E_R)\} + C_L T_{L1}[E_R(2x-1)-x]}{C_L\{[E_R(2x-1)-x] - E_L x(2E_R-1)\}} \quad (59)$$

When $E_{H1} = 0$, Equations (35)–(38) are simplified into $\overline{W}$, η, $\overline{P}$ and $\overline{E}$ of a closed irreversible regenerative BCY coupled to VTHRs. When $E_{H1} = 0$ and $\eta_c = \eta_t = 1$, Equations (35)–(38) are simplified into $\overline{W}$, η, $\overline{P}$ and $\overline{E}$ of a closed endoreversible regenerative BCY coupled to VTHRs. When $E_{H1} = 0$ and $C_H = C_L \to \infty$, Equations (35)–(38) are simplified into $\overline{W}$, η, $\overline{P}$ and $\overline{E}$ of a closed irreversible regenerative BCY coupled to CTHRs. When $E_{H1} = 0$, $C_H = C_L \to \infty$ and $\eta_c = \eta_t = 1$, Equations (35)–(38) are simplified into $\overline{W}$, η, $\overline{P}$ and $\overline{E}$ of a closed endoreversible regenerative BCY coupled to CTHRs.

3. Single Objective Analysis and Optimization

In numerical calculations, $C_{H1} = 0.6\,\mathrm{kW/K}$, $C_L = C_H = 1.2\,\mathrm{kW/K}$, $T_0 = 300\,\mathrm{K}$, $k = 1.4$, $R_g = 0.287\,\mathrm{kJ/(kg\cdot K)}$, $E_H = E_{H1} = E_L = 0.9$, $C_{wf} = 1\,\mathrm{kW/K}$, $\tau_{H1} = 4.33$, $\tau_{H3} = 5$, $\tau_L = 1$ and $\eta_c = \eta_t = 0.9$ are set. The numerical solution of y is obtained by combining Equations (11), (17) and (29). The numerical solution of y is substituted into Equations (35)–(38) to obtain the numerical solutions of $\overline{W}$, η, $\overline{P}$ and $\overline{E}$.

3.1. Single Objective Analysis

The influences of the effectiveness (E_R) of regenerator on $\overline{W}$, η, $\overline{P}$ and $\overline{E}$, π_t and v_5/v_1 are analyzed under the given π. The relationships of $\overline{W}$ and η, $\overline{P}$ and $\overline{E}$ versus π with different E_R are shown in Figures 3 and 4, respectively. From the two figures, $\overline{W}$, η, $\overline{P}$ and $\overline{E}$ all rise firstly and then fall as π rises, and there are respective optimal values of π to make $\overline{W}$, η, $\overline{P}$ and $\overline{E}$ reach their maximum values, respectively. When $\pi < 12.0$, $\overline{W}$, η, $\overline{P}$ and $\overline{E}$ all increase as E_R increases; when $\pi > 12.0$, $\overline{W}$, η, $\overline{P}$ and $\overline{E}$ all decrease as E_R increases. The maximums of $\overline{W}$, η, $\overline{P}$ and $\overline{E}$ gradually move to the left as E_R increases, and the influence on η among them is the greatest. When $\pi = 12.0$ (i.e., $T_2 = T_6$), increasing π will reduce T_3, which allows the exhaust to carry away more heat.

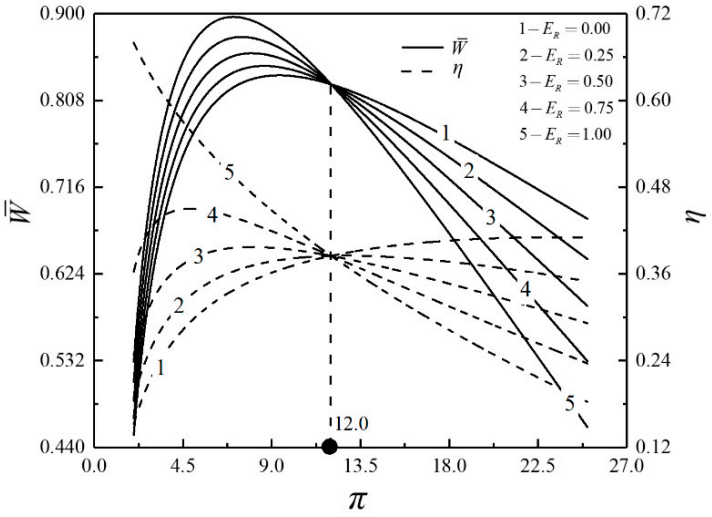

Figure 3. Relationships of $\overline{W}$ and η versus π with different E_R.

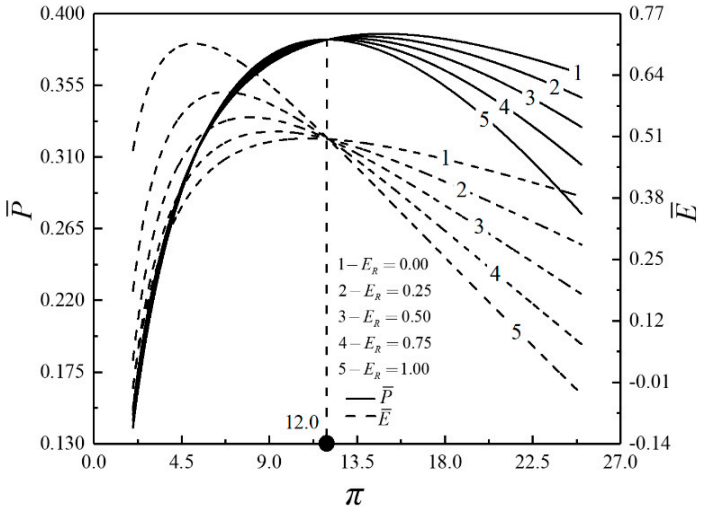

Figure 4. Relationships of $\overline{P}$ and $\overline{E}$ versus π with different E_R.

Figure 5 shows the relationships of π_t and v_5/v_1 versus π with different E_R. From Figure 5, E_R has a great influence on π_t. Given different E_R, the variation rule between π_t and π are different. E_R has a great influence on T_3: when $\pi < 12.0$, π_t increases as E_R increases, which reduces the degree of the isothermal heating; when $\pi > 12.0$, π_t decreases as E_R increases, which aggrandizes the degree of the isothermal heating. v_5/v_1 decreases as π increases. When $\pi < 12.0$, v_5/v_1 increases as E_R increases; when $\pi > 12.0$, v_5/v_1 decreases as E_R increases.

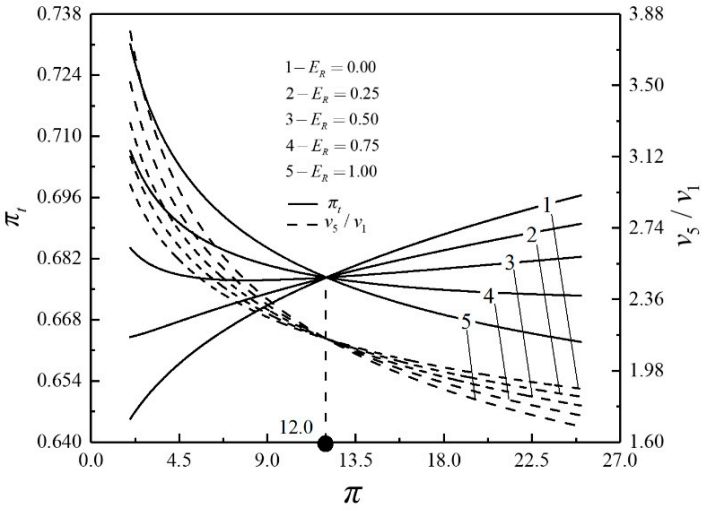

Figure 5. Relationships of π_t and v_5/v_1 versus π with different E_R.

Figure 6 shows the relationships of $\overline{W}$ and η versus π with different η_c and η_t. Figure 7 shows the relationships of $\overline{P}$ and $\overline{E}$ versus π with different η_c and η_t. It can be seen from the figure that $\overline{W}$, η, $\overline{P}$ and $\overline{E}$ increase as η_c or η_t increases. As π increase, η_c or η_t has a greater influence on $\overline{W}$, η, $\overline{P}$ and $\overline{E}$. When $\eta_c = \eta_t = 1$, the cycle is endoreversible, that is, the irreversibilities in the compressor and turbine is not considered. Figure 8 shows the relationships of π_t and v_5/v_1 versus π with different η_c and η_t. It can be seen from the figure that π_t and v_5/v_1 decrease as η_c or η_t increases. It indicates that the degree of the cycle's isothermal heating correction is improved and the volume of the cycle device is reduced by reducing the irreversibility of the cycle.

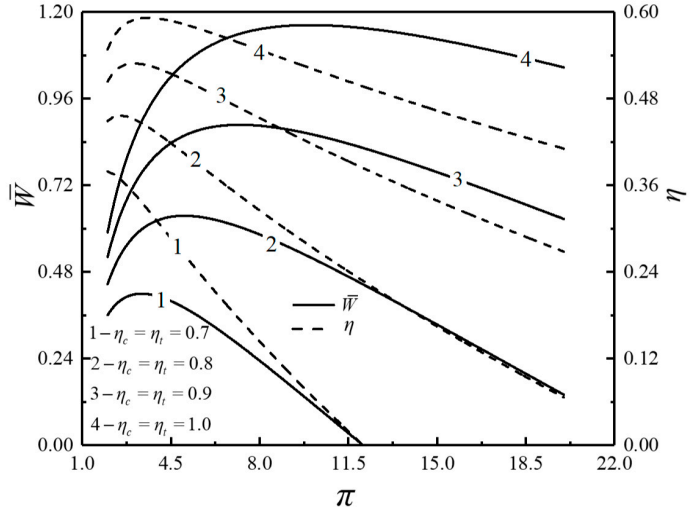

Figure 6. Relationships of $\overline{W}$ and η versus π with different η_c and η_t.

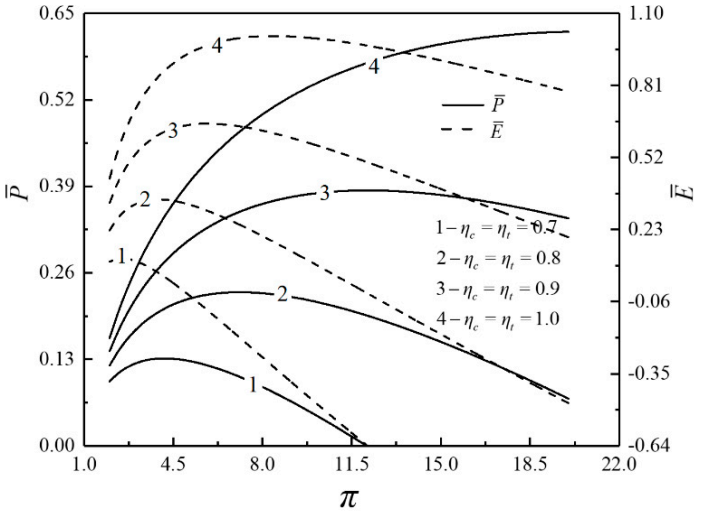

Figure 7. Relationships of $\overline{P}$ and $\overline{E}$ versus π with different η_c and η_t.

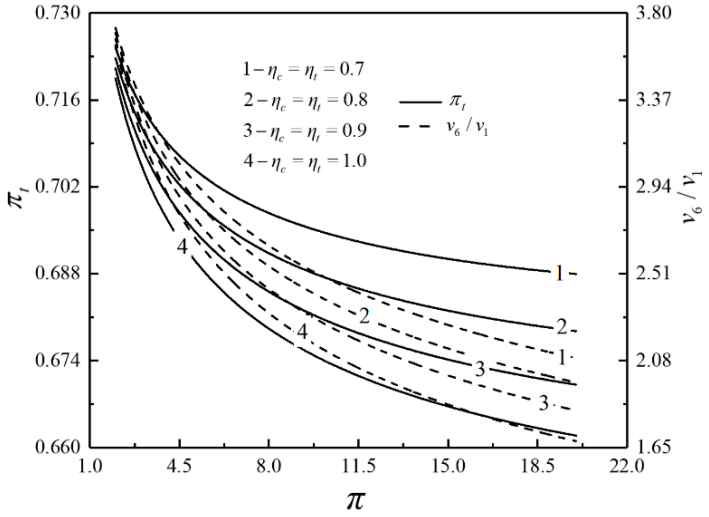

Figure 8. Relationships of π_t and v_5/v_1 versus π with different η_c and η_t.

3.2. Single Objective Optimization

3.2.1. Optimal Distributions of Heat Exchanger Inventory

In the actual design process, the heat exchanger inventory is limited or given, which indicates that the total heat conductance (U_T) is limited or given. According to Equations (35)–(38), $\overline{W}$, η, $\overline{P}$ and $\overline{E}$ are related to U_H, U_{H1}, U_L and U_R. When U_T is given, the reasonable distribution of the heat conductances is conducive to improving the cycle performance. With fixed total heat conductance $U_T(= U_H + U_{H1} + U_L + U_R)$, the HCDs among the RCC, CCC, precooler and regenerator are:

$$u_H = U_H/U_T,\ u_{H1} = U_{H1}/U_T,\ u_L = U_L/U_T,\ u_R = U_R/U_T \tag{60}$$

The HCDs satisfy the following relationships:

$$u_H + u_{H1} + u_L + u_R = 1 \tag{61}$$

$$0 \le u_H,\ u_{H1},\ u_L,\ u_R < 1 \tag{62}$$

With a given U_T, the HCDs are optimized to maximize $\overline{W}$, η, $\overline{P}$ and $\overline{E}$. Figure 9 presents the optimization flowchart for single objective. The optimization calculations of different objectives are similar. Therefore, only the optimization results of $\overline{P}$ is taken as an example for discussions. The optimization results of $\overline{W}$, η and $\overline{E}$ are not presented herein.

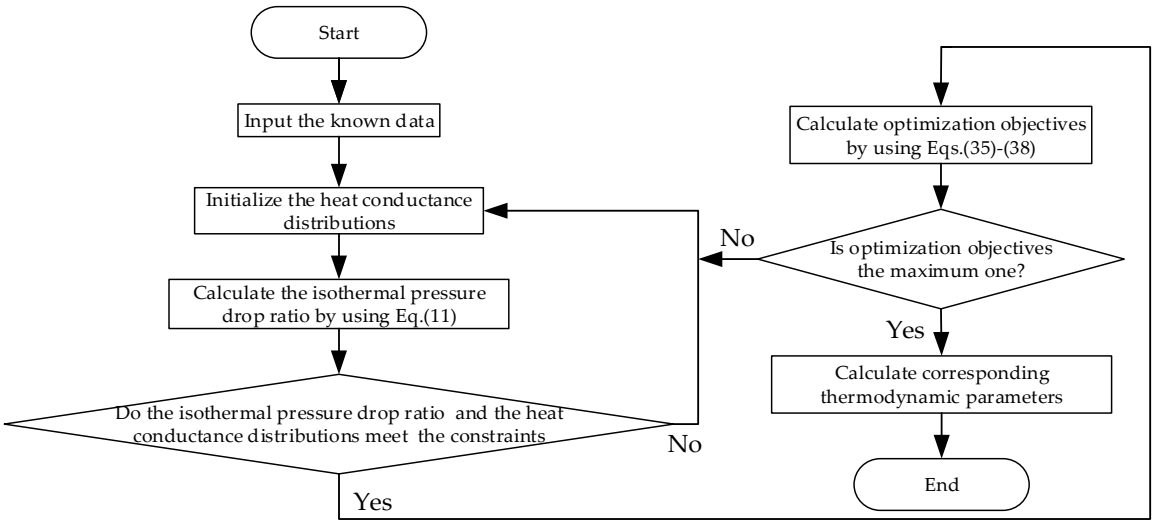

Figure 9. Optimization flowchart for single objective.

Figures 10–12 present the relationships of the maximum power density ($\overline{P}_{\text{opt}}$) and the corresponding power ($\overline{W}_{\overline{P}_{\text{opt}}}$), TEF ($\eta_{\overline{P}_{\text{opt}}}$), ecological function ($\overline{E}_{\overline{P}_{\text{opt}}}$), and other optimal parameters $(\pi_t)_{\overline{P}_{\text{opt}}}$, $(u_H)_{\overline{P}_{\text{opt}}}$, $(u_{H1})_{\overline{P}_{\text{opt}}}$, $(u_L)_{\overline{P}_{\text{opt}}}$ and $(u_R)_{\overline{P}_{\text{opt}}}$ versus π. From Figure 10, $\overline{W}_{\overline{P}_{\text{opt}}}$ and $\overline{P}_{\text{opt}}$ increase first and then decrease as π increases. When $\pi \le 9.2$, $\eta_{\overline{P}_{\text{opt}}}$ first augments and then slightly decreases as π augments; When $\pi > 9.2$, $\eta_{\overline{P}_{\text{opt}}}$ first augments and then decreases as π augments.

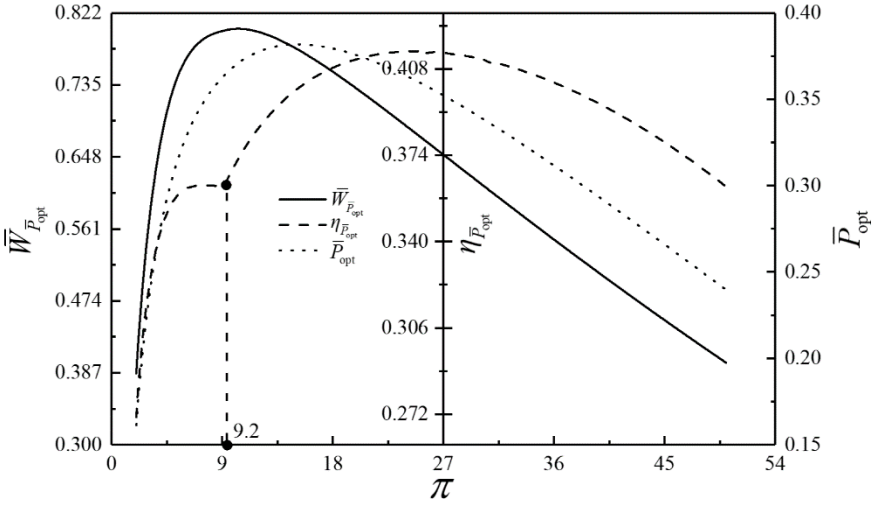

Figure 10. Relationships of $\overline{W}_{\overline{P}_{\text{opt}}}$, $\eta_{\overline{P}_{\text{opt}}}$ and $\overline{P}_{\text{opt}}$ versus π.

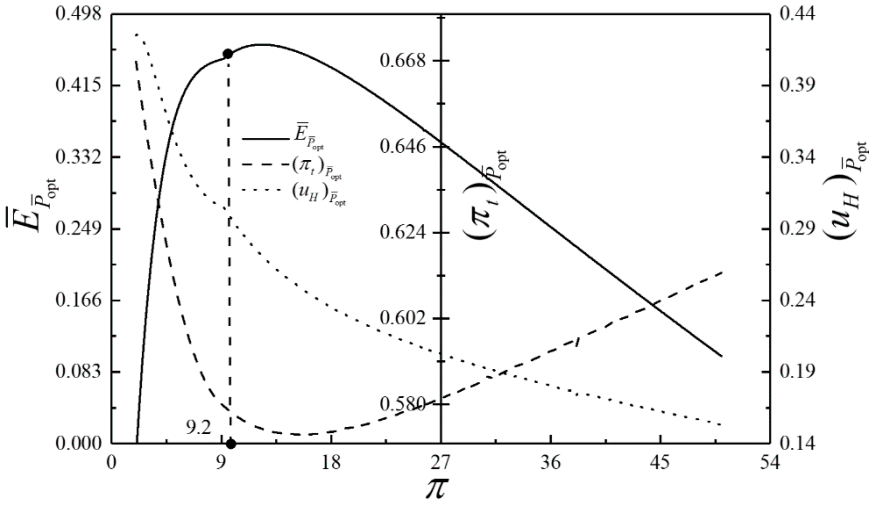

Figure 11. Relationships of $\overline{E}_{\overline{P}_{\text{opt}}}$, $(\pi_t)_{\overline{P}_{\text{opt}}}$ and $(u_H)_{\overline{P}_{\text{opt}}}$ versus π.

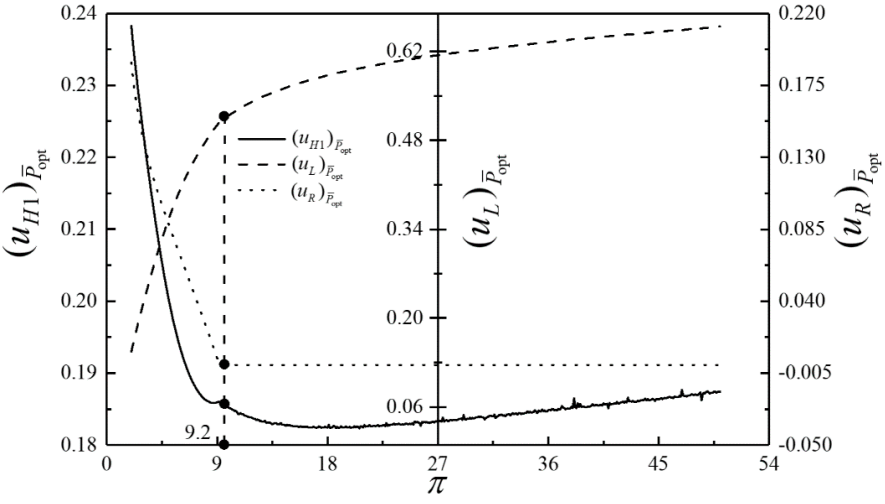

Figure 12. Relationships of $(u_{H1})_{\overline{P}_{\text{opt}}}$, $(u_L)_{\overline{P}_{\text{opt}}}$ and $(u_R)_{\overline{P}_{\text{opt}}}$ versus π.

From Figure 11, when $\pi \leq 9.2$, $\overline{E}_{\overline{P}_{\text{opt}}}$ augments first and then slightly augments as π augments; when $\pi > 9.2$, $\overline{E}_{\overline{P}_{\text{opt}}}$ augments first and then slightly decreases as π augments. $(\pi_t)_{\overline{P}_{\text{opt}}}$ first decreases and then augments as π augments, and the degree of the isothermal heating first augments and then decreases. $(u_H)_{\overline{P}_{\text{opt}}}$ decreases as π augments. From Figure 12, when $\pi \leq 9.2$ and π increases, $(u_{H1})_{\overline{P}_{\text{opt}}}$ diminishes first and then increases slightly, $(u_L)_{\overline{P}_{\text{opt}}}$ increases rapidly, and $(u_R)_{\overline{P}_{\text{opt}}}$ drops rapidly; when $\pi > 9.2$ and π increases, $(u_{H1})_{\overline{P}_{\text{opt}}}$ decreases first and then increases, $(u_L)_{\overline{P}_{\text{opt}}}$ slowly increases, and $(u_R)_{\overline{P}_{\text{opt}}}$ is always 0.

In combination with the previous performance analysis, the regenerator is meaningless when π exceeds a certain value. In this case, E_R should be 0, and the cycle is simplified to a closed irreversible modified simple BCY with an IHP and coupled to VTHRs. In short, the effect of the regenerator is better when π is relatively small; it is not recommended to add a regenerator to the cycle when π is relatively large.

3.2.2. Optimal Thermal Capacitance Rate Matching among the WF and Heat Reservoir

The influences of the thermal capacitance rate matching among the WF and heat reservoir on the cycle performance are discussed. Figure 13 illustrates the relationships of $\overline{P}_{\text{opt}}$ versus C_H/C_{wf} and C_{H1}/C_{wf} when $\pi = 8$. The figure shows that $\overline{P}_{\text{opt}}$ first increases and then tends to remain constant as C_H/C_{wf} increases. Because when $C_H < C_{wf}$, $C_{H\max} = C_{wf}$ and $C_{H\min} = C_H$; when $C_H > C_{wf}$, $C_{H\max} = C_H$ and $C_{H\min} = C_{wf}$; $\overline{P}_{\text{opt}}$ first increases and then tends to remain constant as C_{H1}/C_{wf} increases. Because $\dot{Q}_{3-4}$ first increases and then tends to remain constant as C_{H1}/C_{wf} increases. To further increase the DPD, it is necessary to increase $\dot{Q}_{2-3}$, that is, to increase u_H or U_H. But as $\dot{Q}_{2-3}$ increases, $\dot{Q}_{3-4}$ will also increase, which forms a balance between the two. Finally, the DPD tends to remain constant. By numerical calculations, $\overline{W}_{\overline{P}_{\text{opt}}}$, $\eta_{\overline{P}_{\text{opt}}}$ and $\overline{E}_{\overline{P}_{\text{opt}}}$ also first increase and then tend to remain constants as C_H/C_{wf} or C_{H1}/C_{wf} increases. Thus, there is an optimal C_H/C_{wf} or C_{H1}/C_{wf} to make $\overline{W}_{\overline{P}_{\text{opt}}}$, $\eta_{\overline{P}_{\text{opt}}}$, $\overline{P}_{\text{opt}}$ and $\overline{E}_{\overline{P}_{\text{opt}}}$ to reach the optimal values.

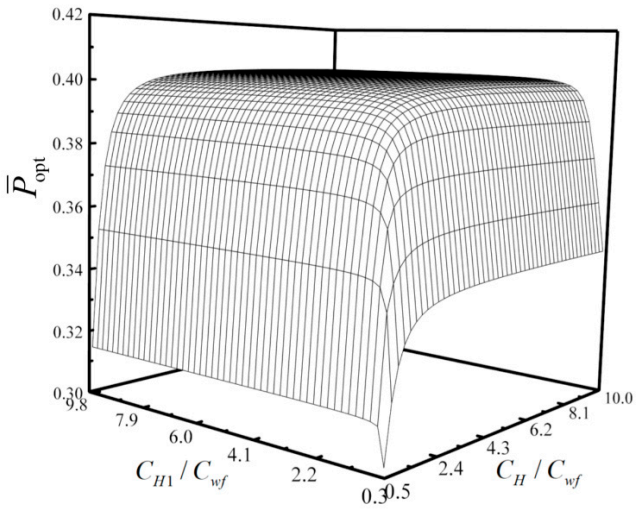

Figure 13. Relationships of $\overline{P}_{\text{opt}}$ versus C_H/C_{wf} and C_{H1}/C_{wf}.

Figure 14 illustrates the relationship of $\overline{P}_{\text{opt}}$ versus C_H/C_{wf} with different C_L/C_H. Figure 15 illustrates the relationship of $\overline{P}_{\text{opt}}$ versus C_{H1}/C_{wf} with different C_L/C_{H1}. As can be seen from the figures, when C_H/C_{wf} or C_{H1}/C_{wf} is smaller, $\overline{P}_{\text{opt}}$ increases as C_L/C_H or C_L/C_{H1} increases; when C_H/C_{wf} or C_{H1}/C_{wf} is larger, $\overline{P}_{\text{opt}}$ is unaffected by C_L/C_H or C_L/C_{H1}. By adjusting the value of C_L/C_H or C_L/C_{H1}, the value of C_H/C_{wf} or C_{H1}/C_{wf} could be changed when $\overline{P}_{\text{opt}}$ reaches the optimal

values. Under the condition that the DPD is kept constant, the requirement of the heat exchangers corresponding to the high-temperature reservoirs can be reduced by increasing C_L/C_H or C_L/C_{H1} and reducing C_H/C_{wf} or C_{H1}/C_{wf}.

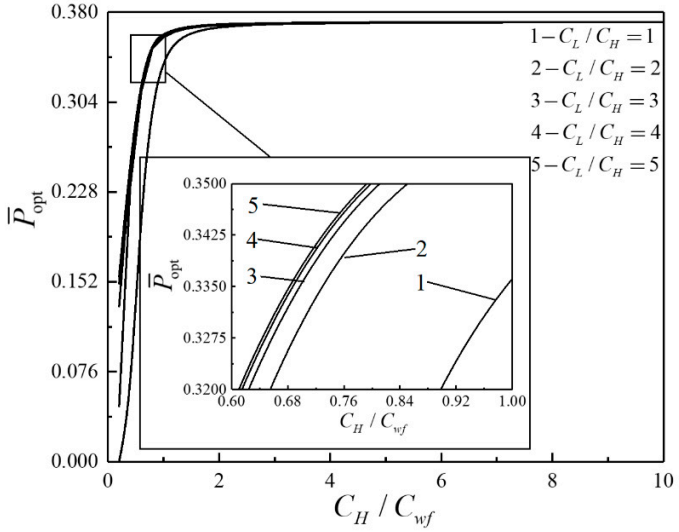

Figure 14. Relationship of $\overline{P}_{opt}$ versus C_H/C_{wf} with different C_L/C_H.

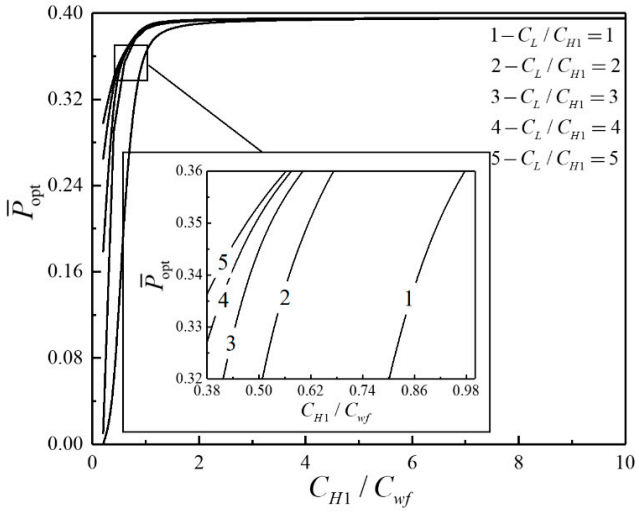

Figure 15. Relationship of $\overline{P}_{opt}$ versus C_{H1}/C_{wf} with different C_L/C_{H1}.

4. Multi-Objective Optimization

Figure 16 shows the optimization flowchart for calculating the Pareto frontier using the NSGA-II algorithm [39–41,45–54]. With π and HCDs as the design variables and $\overline{W}$, η, $\overline{P}$ and $\overline{E}$ as the optimization objectives, the cycle's double, triple or quadruple objective optimization is conducted.

The Pareto frontier contains many feasible solutions, which need to be selected by some methods. The LINMAP, TOPSIS and Shannon entropy methods are three common decision-making methods [40]. These three methods are used to get the optimal scheme from the Pareto frontier, and the results are compared. Finally, the merits and demerits of each decision method are judged by the deviation index (D). Positive ideal point (PIP) is the optimal value combination of four objective functions in the Pareto frontier while negative ideal point (NIP) is the worst value combination. The LINMAP method, TOPSIS method and D are all based on the PIP and NIP.

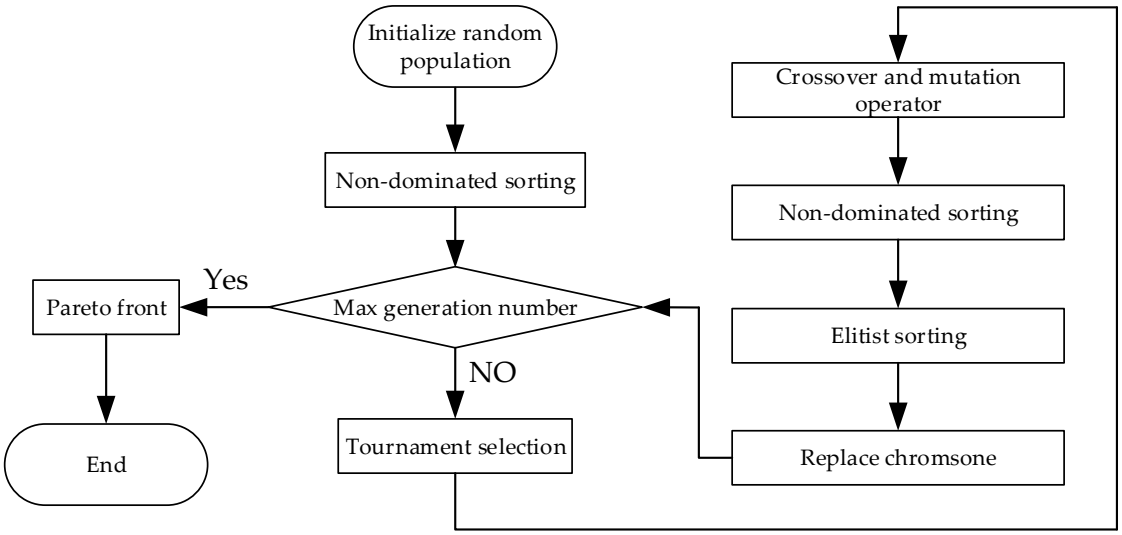

Figure 16. Flowchart of NSGA-II algorithm [40,41,45–51].

For the Shannon entropy method, it is assumed that the Pareto frontier contains n feasible solutions, and each feasible solution contains m objectives. F_{ij} $(1 \le i \le m, 1 \le j \le n)$ represents the value of the j-th optimization objective for the i-th feasible solution, and i_{opt} is the best possible solution in Equation (63).

$$i_{opt} \in \min\left\{P_{ij} \cdot w_j\right\} \tag{63}$$

$$P_{ij} = F_{ij} / \sum_{i=1}^{n} F_{ij},\ SE_j = -\frac{1}{\ln n} \sum_{i=1}^{n} P_{ij} \ln P_{ij} \tag{64}$$

$$w_j = (1 - SE_j) / \sum_{j=1}^{n} (1 - SE_j) \tag{65}$$

where P_{ij} represents the dimensionless value of F_{ij}, and SE_j and w_j are the Shannon entropy and the weight of j-th optimization objective, respectively.

For LINMAP method, i_{opt} is the best possible solution in Equation (66).

$$i_{\text{opt}} \in \min\{ED_{i+}\} \tag{66}$$

$$ED_{i+} = \sqrt{\sum_{j=1}^{m} \left(F_{ij} - F_j^{positive}\right)^2} \tag{67}$$

where ED_{i+} represents the Euclidean distance between the i-th feasible solution and the PIP, and $F^{positive}$ represents the value of the PIP.

For the TOPSIS method, i_{opt} is the best possible solution in Equation (68).

$$i_{\text{opt}} \in \max\left\{\frac{ED_{i+}}{ED_{i+} + ED_{i-}}\right\} \tag{68}$$

$$ED_{i-} = \sqrt{\sum_{j=1}^{m} \left(F_{ij} - F_j^{negative}\right)^2} \tag{69}$$

where ED_{i-} represents the distance between the i-th feasible solution and the NIP, and $F^{negative}$ represents the value of the NIP.

The deviation index is calculated according to Equation (70):

$$D = \frac{\sqrt{\sum_{j=1}^{m} \left(G_j - F_j^{positive}\right)^2}}{\sqrt{\sum_{j=1}^{m} \left(G_j - F_j^{positive}\right)^2} + \sqrt{\sum_{j=1}^{m} \left(G_j - F_j^{negative}\right)^2}} \tag{70}$$

where G_j represents the value of the j-th optimization objective corresponding to the decision method.

Figure 17 shows the Pareto frontier with $\overline{W}$, η, $\overline{P}$ and $\overline{E}$ as the optimization objectives. The line's color of the Pareto frontier represents the value of the DEF. Table 1 lists the comparison of double, triple and quadruple objective optimization results. For quadruple objective optimization, the results gained by LINMAP and TOPSIS methods are the same, and D is smaller than that gained by the Shannon entropy method. It indicates that the results gained by the LINMAP method are better than those gained by the Shannon entropy method. The u_R gained by LINMAP or TOPSIS method is extremely small and tends to 0. The IPDRs of the three decision methods have little difference, thus the isothermal heating degrees of the three methods have little difference. $\overline{W}$ and $\overline{P}$ gained by LINMAP or TOPSIS method are larger than those gained by the Shannon entropy method, but η and $\overline{E}$ gained by LINMAP or TOPSIS method are smaller than those gained by Shannon entropy method. For triple objective optimization, the results gained by LINMAP and TOPSIS methods are the same. The triple objective ($\overline{W}$, $\overline{P}$ and $\overline{E}$) optimization' deviation index gained by LINMAP or TOPSIS method is the smallest. For double objective optimization, all of u_R corresponding to the double objective optimization are extremely small and tend to 0.

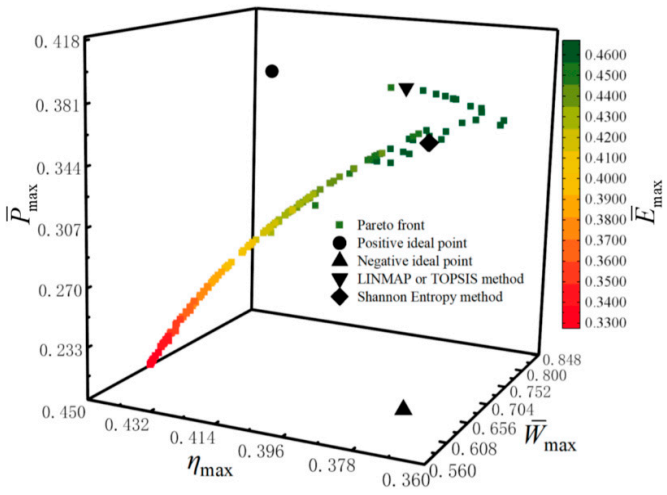

Figure 17. Pareto frontier with $\overline{W}$, η, $\overline{P}$ and $\overline{E}$ as the optimization objectives.

Table 1. Comparison of double, triple and quadruple objective optimization's results.

Optimization Methods	Decision Methods	Optimization Variables					Performance Indexes				Deviation Index	IPDR
		u_H	u_{H1}	u_R	u_L	π	$\bar{W}_{max}$	η_{max}	$\bar{P}_{max}$	$\bar{E}_{max}$	D	π_t
Quadruple objective ($\overline{W}$, η, $\overline{P}$ and $\overline{E}$) optimization	LINMAP	0.251	0.180	0.002	0.567	14.009	0.786	0.395	0.381	0.458	0.259	0.567
	TOPSIS	0.251	0.180	0.002	0.567	14.009	0.786	0.395	0.381	0.458	0.259	0.567
	Shannon Entropy	0.236	0.142	0.106	0.517	7.480	0.799	0.390	0.344	0.467	0.283	0.563
Triple objective ($\overline{W}$, η and $\overline{P}$) optimization	LINMAP	0.234	0.172	0.003	0.591	14.596	0.782	0.397	0.381	0.455	0.268	0.559
	TOPSIS	0.234	0.172	0.003	0.591	14.596	0.782	0.397	0.381	0.455	0.268	0.559
	Shannon Entropy	0.221	0.142	0.115	0.522	7.316	0.798	0.392	0.341	0.466	0.285	0.552
Triple objective ($\overline{W}$, η and $\overline{E}$) optimization	LINMAP	0.197	0.162	0.0009	0.641	13.909	0.786	0.397	0.378	0.457	0.254	0.530
	TOPSIS	0.197	0.162	0.0009	0.641	13.909	0.786	0.397	0.378	0.457	0.254	0.530
	Shannon Entropy	0.224	0.139	0.103	0.534	7.644	0.799	0.390	0.345	0.466	0.281	0.554
Triple objective ($\overline{W}$, $\overline{P}$ and $\overline{E}$) optimization	LINMAP	**0.248**	**0.166**	**0.0002**	**0.586**	**13.643**	**0.792**	**0.395**	**0.380**	**0.463**	**0.237**	**0.568**
	TOPSIS	**0.248**	**0.166**	**0.0002**	**0.586**	**13.643**	**0.792**	**0.395**	**0.380**	**0.463**	**0.237**	**0.568**
	Shannon Entropy	0.241	0.153	0.0003	0.606	12.751	0.798	0.391	0.378	0.466	0.238	0.562
Triple objective (η, $\overline{P}$ and $\overline{E}$) optimization	LINMAP	0.262	0.155	0.004	0.580	14.934	0.777	0.397	0.380	0.452	0.291	0.585
	TOPSIS	0.262	0.155	0.004	0.580	14.934	0.777	0.397	0.380	0.452	0.291	0.585
	Shannon Entropy	0.238	0.140	0.103	0.519	7.529	0.799	0.389	0.345	0.467	0.283	0.565
Double objective optimization ($\overline{W}$ and η)	LINMAP	0.208	0.1564	0.0005	0.635	15.225	0.777	0.402	0.380	0.453	0.273	0.547
	TOPSIS	0.209	0.1558	0.0005	0.634	15.119	0.778	0.402	0.379	0.454	0.269	0.548
	Shannon Entropy	0.220	0.147	0.0007	0.631	14.160	0.785	0.398	0.379	0.459	0.250	0.556
Double objective optimization ($\overline{W}$ and $\overline{P}$)	LINMAP	0.245	0.174	0.0007	0.580	12.662	0.798	0.390	0.379	0.465	0.242	0.559
	TOPSIS	0.245	0.174	0.0007	0.580	12.662	0.798	0.390	0.379	0.465	0.242	0.559
	Shannon Entropy	0.247	0.171	0.0006	0.582	11.757	0.804	0.385	0.376	0.466	0.252	0.557
Double objective optimization ($\overline{W}$ and $\overline{E}$)	LINMAP	0.206	0.1486	0.0007	0.646	16.561	0.763	0.406	0.378	0.445	0.335	0.555
	TOPSIS	0.206	0.1486	0.0007	0.646	16.561	0.763	0.406	0.378	0.445	0.335	0.555
	Shannon Entropy	0.206	0.1486	0.0007	0.646	16.561	0.763	0.406	0.378	0.445	0.335	0.555
Double objective optimization (η and $\overline{P}$)	LINMAP	0.207	0.159	0.0007	0.633	21.169	0.715	0.413	0.371	0.406	0.630	0.570
	TOPSIS	0.207	0.159	0.0004	0.634	21.248	0.715	0.414	0.371	0.407	0.624	0.570
	Shannon Entropy	0.208	0.160	0.0005	0.634	21.249	0.715	0.415	0.372	0.408	0.618	0.570
Double objective optimization (η and $\overline{E}$)	LINMAP	0.219	0.162	0.0003	0.619	14.589	0.784	0.400	0.380	0.458	0.247	0.551
	TOPSIS	0.221	0.163	0.0003	0.618	14.293	0.786	0.398	0.380	0.460	0.245	0.551
	Shannon Entropy	0.224	0.160	0.0003	0.616	12.766	0.797	0.391	0.378	0.465	0.240	0.548
Double objective optimization ($\overline{P}$ and $\overline{E}$)	LINMAP	0.198	0.174	0.0002	0.627	22.134	0.706	0.415	0.369	0.399	0.674	0.563
	TOPSIS	0.198	0.174	0.0002	0.627	22.134	0.706	0.415	0.369	0.399	0.674	0.563
	Shannon Entropy	0.198	0.174	0.0002	0.627	22.134	0.706	0.415	0.369	0.399	0.674	0.563
PIP		——	——	——	——	——	0.809	0.438	0.381	0.467	——	——
NIP		——	——	——	——	——	0.677	0.369	0.360	0.373	——	——

5. Conclusions

FTT is applied to establish a model of a closed irreversible regenerative BCY with an IHP and variable IPDR in this paper. The DPO, TEF, DPD and DEF are obtained, and the influences of E_R on the performance indexes are analyzed. With $\overline{P}$ as the optimization objective and HCDs as the design variables, the single objective analysis and optimization of the cycle are conducted. Based on the NSGA-II algorithm, the DPO, TEF, DPD and DEF are maximized with π and HCDs as the design variables and the corresponding Pareto frontier is obtained. Three decision methods are applied to get the best scheme. The main conclusions manifest that:

(1) For the single objective analysis, the DPO, TEF, DPD and DEF all augment first and then reduce as π augments. When $\pi < 12.0$, it is beneficial to add the regenerator to improve the cycle performance; when $\pi > 12.0$, adding the regenerator will reduce the cycle performance. For the single-objective optimization, when $\pi > 9.2$, the effectiveness at the regenerator should be 0, and the cycle will be simplified into a closed irreversible modified BCY with an IHP and coupled to VTHRs. Hence, the regenerator is added, and a suitable pressure ratio should be selected in the limited range. In the actual process, the pressure ratio should be strictly controlled in this new-type gas turbine, or the new-type gas turbine is suitable for the situations where the pressure ratio is relatively low. The DPO, TEF, DPD and DEF increase as η_c or η_t increases. π_t and v_5/v_1 decrease as η_c or η_t increases. It indicates that the cycle performance and the degree of the cycle's isothermal heating correction are improved and the volume of the cycle device is reduced by reducing the irreversibility of the cycle.

(2) For the quadruple objective optimization, the results gained by LINMAP and TOPSIS methods are the same, and D is smaller than that gained by the Shannon entropy method. Therefore, the results gained by LINMAP and TOPSIS methods are better than those gained by the Shannon entropy method. For the double, triple or quadruple objective optimization, the triple objective ($\overline{W}$, $\overline{P}$ and $\overline{E}$) optimization' deviation index gained by LINMAP or TOPSIS method is the smallest. According to decision-makers' actual needs, they could choose the best scheme from the Pareto frontier, design the new-type gas turbine reasonably, and then determine the construction or the operation of the gas turbine.

FTT is a powerful theoretical tool and the NSGA-II algorithm is an effective mathematical tool for the performance analysis and optimization of closed irreversible regenerative BCY with an IHP and variable IPDR. The results obtained in this paper have some guiding significance for the design of a new-type gas turbine.

Author Contributions: Conceptualization, L.C. and C.T.; Funding acquisition, L.C.; Methodology, L.C. and C.T.; Software, C.T., H.F., and Y.G.; Supervision, L.C.; Validation, C.T. and Y.G.; Writing—original draft, C.T. and H.F.; Writing—review & editing, L.C. All authors have read and approved the final manuscript.

Funding: This research was funded by the National Natural Science Foundation of China (Grant No. 51779262) and the Innovation Research Foundation for Master Candidates of Naval University of Engineering, P. R. China (Grant No. HGCXJJ2019009).

Acknowledgments: The authors wish to thank the reviewers for their careful, unbiased and constructive suggestions, which led to this revised manuscript.

Conflicts of Interest: The authors declare no conflict of interest.

Nomenclature

C	Thermal capacitance rate (kW/K)
E	Effectiveness, ecological function (kW/K)
$\overline{E}$	Dimensionless ecological function
$\overline{P}$	Dimensionless power density
T	Temperature (K)
U	Heat conductance (kW/K)
u	Heat conductance distribution
$\overline{W}$	Dimensionless power output
Greek symbol	
η	Efficiency
π	Pressure ratio
τ	Temperature ratio
Subscripts	
H	Heat exchanger at the regular combustion chamber
$H1$	Heat exchanger at the converging combustion chamber
L	Cold-side heat exchanger at the precooler
wf	Working fluid
1-7,2s,6s	State points

Abbreviations

BCY	Brayton cycle
CCC	Converging combustion chamber
CTHR	Constant-temperature heat reservoir
DEF	Dimensionless ecological function
DPD	Dimensionless power density
DPO	Dimensionless power output
FTT	Finite-time thermodynamics
HCD	Heat conductance distribution
IHP	Isothermal heating process
IPDR	Isothermal pressure drop ratio
NIP	Negative ideal point
PIP	Positive ideal point
RCC	Regular combustion chamber
TEF	Thermal efficiency
VTHR	Variable-temperature heat reservoir
WF	Working fluid

References

1. Vecchiarelli, J.; Kawall, J.G.; Wallace, J.S. Analysis of a concept for increasing the efficiency of a Brayton cycle via isothermal heat addition. *Int. J. Energy Res.* **1997**, *21*, 113–127. [CrossRef]
2. Göktun, S.; Yavuz, H. Thermal efficiency of a regenerative Brayton cycle with isothermal heat addition. *Energy Convers. Manag.* **1999**, *40*, 1259–1266. [CrossRef]
3. Erbay, L.B.; Göktun, S.; Yavuz, H. Optimal design of the regenerative gas turbine engine with isothermal heat addition. *Appl. Energy* **2001**, *68*, 249–264. [CrossRef]
4. Jubeh, N.M. Exergy analysis and second law efficiency of a regenerative Brayton cycle with isothermal heat addition. *Entropy* **2005**, *7*, 172–187. [CrossRef]
5. El-Maksound, R.M.A. Binary Brayton cycle with two isothermal processes. *Energy Convers. Manag.* **2013**, *73*, 303–308. [CrossRef]
6. Andresen, B.; Salamon, P.; Berry, R.S. Thermodynamics in finite time. *Phys. Today* **1987**, *37*, 62–70. [CrossRef]
7. Berry, R.S.; Kazakov, V.A.; Sieniutycz, S.; Szwast, Z.; Tsirlin, A.M. *Thermodynamic Optimization of Finite Time Processes*; Wiley: Chichester, UK, 1999.

8. Dincer, I.; Zamfirescu, C. *Advanced Power Generation Systems*; Elsevier: London, UK, 2014.
9. Perescu, S.; Costea, M.; Feidt, M.; Ganea, I.; Boriaru, N. *Advanced Thermodynamics of Irreversible Processes with Finite Speed and Finite Dimensions*; Editura AGIR: Bucharest, Romania, 2015.
10. Kaushik, S.C.; Tyagi, S.K.; Kumar, P. *Finite Time Thermodynamics of Power and Refrigeration Cycles*; Springer: New York, NY, USA, 2018.
11. Sieniutycz, S. *Complexity and Complex Thermo-Economic Systems*; Elsevier: Amsterdam, The Netherlands, 2020.
12. Chen, L.G.; Wu, C.; Sun, F.R. Finite time thermodynamic optimization or entropy generation minimization of energy systems. *J. Non-Equilib. Thermodyn.* **1999**, *24*, 327–359. [CrossRef]
13. Andresen, B. Current trends in finite-time thermodynamics. *Angew. Chem. Int. Edition.* **2011**, *50*, 2690–2704. [CrossRef]
14. Roach, T.N.F.; Salamon, P.; Nulton, J.; Andresen, B.; Felts, B.; Haas, A.; Calhoun, S.; Robinett, N.; Rohwer, F. Application of finite-time and control thermodynamics to biological processes at multiple scales. *J. Non-Equilib. Thermodyn.* **2018**, *43*, 193–210. [CrossRef]
15. Feidt, M.; Costea, M. Progress in Carnot and Chambadal modeling of thermomechanical engine by considering entropy and heat transfer entropy. *Entropy* **2019**, *21*, 1232. [CrossRef]
16. Atmaca, M.; Gumus, M. Power and efficiency analysis of Diesel cycle under alternative criteria. *Arab. J. Sci. Eng.* **2014**, *39*, 2263–2270. [CrossRef]
17. Chen, L.G.; Liu, X.W.; Wu, F.; Feng, H.J.; Xia, S.J. Power and efficiency optimization of an irreversible quantum Carnot heat engine working with harmonic oscillators. *Physica A* **2020**, *550*, 124140. [CrossRef]
18. Chen, L.G.; Shen, J.F.; Ge, Y.L.; Wu, Z.X.; Wang, W.H.; Zhu, F.L.; Feng, H.J. Power and efficiency optimization of open Maisotsenko-Brayton cycle and performance comparison with traditional open regenerated Brayton cycle. *Energy Convers. Manag.* **2020**, *217*, 113001. [CrossRef]
19. Sahin, B.; Kodal, A.; Yavuz, H. Maximum power density analysis of an endoreversible Carnot heat engine. *Energy* **1996**, *21*, 1219–1225. [CrossRef]
20. Chen, L.G.; Zheng, J.L.; Sun, F.R.; Wu, C. Optimum distribution of heat exchanger inventory for power density optimization of an endoreversible closed Brayton cycle. *J. Phys. D Appl. Phys.* **2001**, *34*, 422–427. [CrossRef]
21. Chen, L.G.; Zheng, J.L.; Sun, F.R.; Wu, C. Performance comparison of an endoreversible closed variable-temperature heat reservoir Brayton cycle under maximum power density and maximum power conditions. *Energy Convers. Manag.* **2002**, *43*, 33–43. [CrossRef]
22. Chen, L.G.; Zheng, J.L.; Sun, F.R.; Wu, C. Power density optimization for an irreversible closed Brayton cycle. *Open Syst. Inf. Dyn.* **2001**, *8*, 241–260. [CrossRef]
23. Chen, L.G.; Zheng, J.L.; Sun, F.R.; Wu, C. Performance comparison of an irreversible closed variable-temperature heat reservoir Brayton cycle under maximum power density and maximum power conditions. *Proc. IMechE Part A J. Power and Energy* **2005**, *219*, 559–566. [CrossRef]
24. Angulo-Brown, F. An ecological optimization criterion for finite-time heat engines. *Eur. J. Appl. Physiol.* **1991**, *69*, 7465–7469. [CrossRef]
25. Yan, Z.J. Comment on "ecological optimization criterion for finite-time heat engines". *Eur. J. Appl. Physiol.* **1993**, *73*, 3583.
26. Chen, L.G.; Sun, F.R.; Chen, W.Z. The ecological quality factor for thermodynamic cycles. *J. Eng. Therm. Energy Power.* **1994**, *9*, 374–376. (In Chinese)
27. Ma, Z.S.; Chen, Y.; Wu, J.H. Ecological optimization for a combined diesel-organic Rankine cycle. *AIP Adv.* **2019**, *9*, 015320. [CrossRef]
28. Chen, L.G.; Liu, X.W.; Wu, F.; Xia, S.J.; Feng, H.J. Exergy-based ecological optimization of an irreversible quantum Carnot heat pump with harmonic oscillators. *Physica A* **2020**, *537*, 122597. [CrossRef]
29. Kaushik, S.C.; Tyagi, S.K.; Singhal, M.K. Parametric study of an irreversible regenerative Brayton cycle with isothermal heat addition. *Energy Convers. Manag.* **2003**, *44*, 2013–2025. [CrossRef]
30. Tyagi, S.K.; Kaushik, S.C.; Tiwari, V. Ecological optimization and parametric study of an irreversible regenerative modified Brayton cycle with isothermal heat addition. *Entropy* **2003**, *5*, 377–390. [CrossRef]
31. Tyagi, S.K.; Chen, J.; Kaushik, S.C. Optimum criteria based on the ecological function of an irreversible intercooled regenerative modified Brayton cycle. *Int. J. Exergy* **2005**, *2*, 90–107. [CrossRef]
32. Tyagi, S.K.; Chen, J. Performance evaluation of an irreversible regenerative modified Brayton heat engine based on the thermoeconomic criterion. *Int. J. Power Energy Syst.* **2006**, *26*, 66–74. [CrossRef]

33. Tyagi, S.K.; Chen, J.; Kaushik, S.C.; Wu, C. Effects of intercooling on the performance of an irreversible regenerative modified Brayton cycle. *Int. J. Power Energy Syst.* **2007**, *27*, 256–264. [CrossRef]
34. Tyagi, S.K.; Wang, S.; Kaushik, S.C. Irreversible modified complex Brayton cycle under maximum economic condition. *Indian J. Pure Appl. Phys.* **2006**, *44*, 592–601.
35. Tyagi, S.K.; Wang, S.; Park, S.R. Performance criteria on different pressure ratios of an irreversible modified complex Brayton cycle. *Indian J. Pure Appl. Phys.* **2008**, *46*, 565–574.
36. Kumar, R.; Kaushik, S.C.; Kumar, R. Power optimization of an irreversible regenerative Brayton cycle with isothermal heat addition. *J. Therm. Eng.* **2015**, *1*, 279–286. [CrossRef]
37. Wang, J.H.; Chen, L.G.; Ge, Y.L.; Sun, F.R. Power and power density analyzes of an endoreversible modified variable-temperature reservoir Brayton cycle with isothermal heat addition. *Int. J. Low-Carbon Technol.* **2016**, *11*, 42–53. [CrossRef]
38. Wang, J.H.; Chen, L.G.; Ge, Y.L.; Sun, F.R. Ecological performance analysis of an endoreversible modified Brayton cycle. *Int. J. Sustain. Energy* **2014**, *33*, 619–634. [CrossRef]
39. Tang, C.Q.; Chen, L.G.; Wang, W.H.; Feng, H.J.; Xia, S.J. Performance optimization of the endoreversible simple MCBC coupled to variable-temperature reservoirs based on NSGA-II algorithm. *Power Gener. Technol.* **2020**, *41*, 301–306. (In Chinese)
40. Tang, C.Q.; Feng, H.J.; Chen, L.G.; Wang, W.H. Power density analysis and multi-objective optimization for a modified endoreversible simple closed Brayton cycle with one isothermal heating process. *Energy Rep.* **2020**, *6*, 1648–1657. [CrossRef]
41. Arora, R.; Kaushik, S.C.; Kumar, R.; Arora, R. Soft computing based multi-objective optimization of Brayton cycle power plant with isothermal heat addition using evolutionary algorithm and decision making. *Appl. Soft Comput.* **2016**, *46*, 267–283. [CrossRef]
42. Arora, R.; Arora, R. Thermodynamic optimization of an irreversible regenerated Brayton heat engine using modified ecological criteria. *J. Therm. Eng.* **2020**, *6*, 28–42. [CrossRef]
43. Qi, W.; Wang, W.H.; Chen, L.G. Power and efficiency performance analyses for a closed endoreversible binary Brayton cycle with two isothermal processes. *Therm. Sci. Eng. Prog.* **2018**, *7*, 131–137. [CrossRef]
44. Tang, C.Q.; Chen, L.G.; Feng, H.J.; Wang, W.H.; Ge, Y.L. Power optimization of a closed binary Brayton cycle with isothermal heating processes and coupled to variable-temperature reservoirs. *Energies* **2020**, *13*, 3212. [CrossRef]
45. Ahmadi, M.H.; Ahmadi, M.A.; Mehrpooya, M.; Hosseinzade, H.; Feidt, M. Thermodynamic and thermo-economic analysis and optimization of performance of irreversible four- temperature-level absorption refrigeration. *Energy Convers. Manag.* **2014**, *88*, 1051–1059. [CrossRef]
46. Arora, R.; Kaushik, S.C.; Arora, R. Multi-objective and multi-parameter optimization of two-stage thermoelectric generator in electrically series and parallel configurations through NSGA-II. *Energy* **2015**, *91*, 242–254. [CrossRef]
47. Sadatsakkak, S.A.; Ahmadi, M.H.; Bayat, R.; Pourkiaei, S.M.; Feidt, M. Optimization density power and thermal efficiency of an endoreversible Braysson cycle by using non-dominated sorting genetic algorithm. *Energy Convers. Manag.* **2015**, *93*, 31–39. [CrossRef]
48. Sadatsakkak, S.A.; Ahmadi, M.H.; Ahmadi, M.A. Thermodynamic and thermo-economic analysis and optimization of an irreversible regenerative closed Brayton cycle. *Energy Convers. Manag.* **2015**, *94*, 124–129. [CrossRef]
49. Sadatsakkak, S.A.; Ahmadi, M.H.; Ahmadi, M.A. Optimization performance and thermodynamic analysis of an irreversible nano scale Brayton cycle operating with Maxwell-Boltzmann gas. *Energy Convers. Manag.* **2015**, *101*, 592–605. [CrossRef]
50. Kumar, R.; Kaushik, S.C.; Kumar, R.; Hans, R. Multi-objective thermodynamic optimization of an irreversible regenerative Brayton cycle using evolutionary algorithm and decision making. *Ain Shams Eng. J.* **2016**, *7*, 741–753. [CrossRef]
51. Valencia, G.; Núñez, J.; Duarte, J. Multiobjective optimization of a plate heat exchanger in a waste heat recovery organic Rankine cycle system for natural gas engines. *Entropy* **2019**, *21*, 655. [CrossRef]
52. Zhang, L.; Chen, L.G.; Xia, S.K.; Ge, Y.L.; Wang, C.; Feng, H.J. Multi-objective optimization for helium-heated reverse water gas shift reactor by using NSGA-II. *Int. J. Heat Mass Transf.* **2020**, *148*, 119025. [CrossRef]

53. Wu, Z.X.; Feng, H.J.; Chen, L.G.; Ge, Y.L. Performance optimization of a condenser in ocean thermal energy conversion (OTEC) system based on constructal theory and multi-objective genetic algorithm. *Entropy* **2020**, *22*, 641. [CrossRef]
54. Sun, M.; Xia, S.J.; Chen, L.G.; Wang, C.; Tang, C.Q. Minimum entropy generation rate and maximum yield optimization of sulfuric acid decomposition process using NSGA-II. *Entropy* **2020**, *22*, 1065. [CrossRef]